Frontiers in Computing and Intelligent Systems
ISSN: 2832-6024 | Vol. 17, No. 1, 2026

An EKF-Based Satellite-Visual-Inertial Integrated Navigation Algorithm for Agricultural Machinery

Yifan Liu, Baofeng Ji, Zhenyun Sun, Saibing Wang, Hongying Wang

Henan University of Science and Technology, Luoyang, Henan, China

Abstract: In order to overcome the limitations of relying on a single sensor in a complex agricultural environment, this paper studies the integration of navigation parameters across satellite, visual and inertial platforms. The different characteristics of these sensors are analyzed in detail to establish the state equation. Based on these mathematical models, an extended Kalman filter (EKF) is designed. Through state estimation and measurement update of different data sets, the efficient synthesis of Global Navigation Satellite System (GNSS), visual recognition module and Inertial Navigation System (INS) information is realized. In addition, MATLAB is used for comparative simulation. The results show that the proposed multi-sensor integrated framework has higher accuracy and robustness than single GNSS and dual GNSS / INS systems. Among them, the east position error is constrained between-0.42 ~ 0.37 m, and the north position error is constrained between-0.22 ~ 0.26 m.

Keywords: Extended Kalman Filter; Agricultural Machinery; Satellite-Visual-Inertial Integrated Navigation Algorithm.

1. Introduction

The main technical methods of automatic navigation for agricultural mechanization include image-based visual navigation, global satellite navigation system, Light Detection and Ranging (LiDAR) navigation and inertial navigation system based on internal sensors. The multi-sensor fusion system applied to robot navigation planning can analyze and synthesize data information from different sensors in multiple levels and multiple spaces to generate a consistent interpretation of the observed environment [1]. Visual sensors can generate environment-related information and build visual maps. However, due to the complexity and uncertainty of the agricultural environment, it is difficult for a single visual sensor to meet the requirements of accurate navigation. The accuracy of visual perception is susceptible to changes in ambient light and weather. In some cases, images may become unreliable, resulting in incorrect navigation planning. In order to overcome these shortcomings, it is necessary to integrate signals with complementary characteristics of other sensors, such as global navigation satellite system, inertial measurement unit (IMU) and lidar, which can effectively improve the performance of visual navigation [2].

Compared with visual sensors, GNSS can provide more accurate spatial coordinates. Laser radar has strong penetration ability for blurred visual occlusions such as dust and trees, and is more stable in light changing environment [3]. However, due to the openness of the outdoor farm environment, SLAM itself under the lidar system only solves the problem of positioning and mapping, and the characteristics of the working process without loopback may affect the positioning accuracy. When the visual sensor cannot obtain effective pose estimation, the IMU sensor can obtain good motion pose estimation in a short time [4]. Compared with the single vision navigation system, the multi-sensor fusion system further improves the environmental perception and navigation ability of agricultural robots and vehicles. The multi-sensor fusion system enriches the information acquisition mode and improves the information acquisition and environmental perception ability in complex agricultural environment [5]. In addition, the multi-sensor fusion system organically combines the visual modal information to improve the positioning accuracy of sensors and other sensors and the robustness of navigation tasks.

Taking into account the multipath effect and signal interference in the urban environment, Sun et al.proposed the integration of inertial measurement unit, Global Positioning System (GPS) and monocular visual odometry (VO) for urban vehicle navigation, and developed an integrated algorithm based on Extended Kalman Filter (EKF). The results show that the three-dimensional root mean square error of the proposed IMU / GPS / VO fusion algorithm is 3.285 meters [6]. Reitbauer et al.integrated GNSS-RTK, IMU and wheel speed sensors in the error state Kalman filter to estimate the position and attitude of the vehicle. The results show that the estimation accuracy of the horizontal position of the vehicle is still sub-10 cm after 30 seconds of GNSS satellite signal interruption. [7] Guohao Zhang and Li-TaHsu proposed an adaptive Kalman filter using fuzzy logic random forest to achieve GNSS accuracy classification, which effectively improved the positioning accuracy of the global navigation satellite system. The overall positioning accuracy of the experimental surface was improved by about 50 % [8].

Most of the existing agricultural machinery navigation methods rely on GNSS / INS fusion technology, which is difficult to achieve autonomous navigation of agricultural machinery when GNSS signals are not available. [9]. Although visual / inertial navigation systems are widely used in the field of autonomous vehicles, most of the solutions are based on the SLAM framework. However, SLAM mainly solves the positioning problem, and navigation also relies on pre-built maps for path planning. Agricultural machinery often does not form a closed loop during field operations, which makes the SLAM system vulnerable to cumulative errors in such non-closed-loop scenarios. Due to these limitations, the navigation solutions of traditional autonomous vehicles are not fully applicable to agricultural autonomous driving equipment [10]. In this paper, an integrated navigation method based on the fusion of satellite, camera and inertial measurement unit based on extended Kalman filter is designed, which overcomes the limitation of

single sensor in the face of complex farmland environment, enhances the adaptability to the environment and improves the navigation accuracy, and provides a more reliable and accurate autonomous navigation solution for agricultural machinery.

In view of the limitations of different sensors in farmland scenes, this paper combines the characteristics of satellite, vision and inertial sensors, and uses IMU attitude, acceleration bias, angular velocity bias, lateral deviation, heading angle deviation, satellite positioning coordinates and three-axis velocity as state variables. The state equation is established, and the data of gyroscope and accelerometer are used as the basis of state transition. Satellite positioning, accelerometer and visual navigation data are used as observation input updates, and data fusion is performed through the designed extended Kalman filter. A series of comparative experiments are designed using Matlab to verify the effectiveness of the fusion strategy in enhancing navigation accuracy and robustness.

2. GNSS Positioning System

The Global Navigation Satellite System (GNSS) is a system consisting of multiple Earth-orbiting satellites designed to provide global users with positioning, navigation, and time signals. Including global, regional and enhanced, such as the United States GPS, Russia 's Glonass, Europe 's Galileo and China 's Beidou satellite navigation system. By receiving signals from at least four satellites, GNSS can provide global users with accurate three-dimensional position (latitude, longitude and altitude) and time information. GNSS technology plays a key role in military, civil aviation, maritime transport, ground transportation, disaster management, scientific research and many other fields [11]. In this paper, China 's BeiDou Navigation Satellite System (BDS) is used to receive satellite signals.

A GNSS typically consists of three primary segments:

Space Segment: It is composed of multiple satellites in the middle earth orbit. These satellites are responsible for transmitting navigation signals containing their position and time information, which constitutes the core of the system.

Control Segment: It includes a ground monitoring station, which is responsible for maintaining the normal operation of the satellite, including monitoring the health status of the satellite, orbital parameters and time synchronization to ensure the accuracy of the transmitted signal. The monitoring station is not only responsible for collecting atmospheric condition data in the environment, but also for processing signals from satellites and their operating status information. These collected data are then transmitted to the control center.

User Segment: It is composed of various GNSS receivers, through which users receive satellite signals and process them to obtain accurate position and time information. The function of the user side focuses on signal reception and navigation calculation, aiming to provide users with the service of receiving data. There are many kinds of GNSS receivers. According to different needs and positioning accuracy requirements, users can choose the appropriate receiver.

The BDS positioning principle is based on the signal propagation time difference between the space satellite and the receiver to determine the position of the receiver. Each Beidou satellite emits signals containing its own position (ephemeris) and launch time information. The receiver receives these signals and measures the signal propagation time from the satellite to the receiver. Assuming the distance between the satellite and the receiver is denoted as d , the signal propagation time is t , and the speed of light is c , the distance can be calculated as $d = c \cdot t$. For each individual satellite, the formula for the receiver to compute its position is expressed as:

$$\left[(x-x_i)^2+(y-y_i)^2+(z-z_i)^2\right]^{1/2} = \left(c\times(t-t_i)\right)^2 \quad (1)$$

Where (x, y, z) is the position of the receiver, (x_i, y_i, z_i) is the position of the *i*-th satellite, t is the time of signal reception, and t_i is the signal transmission time of the *i*-th satellite.

This process is shown in Figure 1, based on a pre-defined control point set on the satellite, which is a reference point for a known location. When the receiver captures signals from multiple satellites, it calculates the position based on the accurate time of each satellite signal transmission, the time point at which the signal is received, and the satellite 's orbital data. This process not only includes direct distance calculation, but also involves the correction of receiver clock error and the consideration of multipath effect to ensure the accuracy of positioning results.

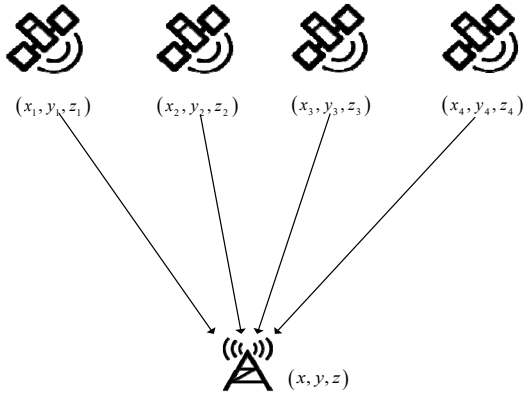

Fig 1. Principle diagram of Beidou satellite positioning

The Beidou system positioning process involves at least four satellites, which are used to solve the three-dimensional position and time deviation of the receiver. The distance from the receiver to each satellite is calculated by the signal propagation time and light speed [12].

In the process of satellite signal propagation, it is affected by various factors such as ionospheric and tropospheric errors, multipath effects, and device errors at the receiver end. These cumulative errors may cause great ranging errors between the receiver and the satellite during the positioning process of the Beidou satellite navigation system, sometimes up to tens or even hundreds of meters, which has a significant negative impact on the positioning accuracy of the system. By using differential technology, especially Real-time Kinematic (RTK) technology, the error caused by signal propagation and satellite clock error can be effectively eliminated, thereby significantly improving the accuracy of positioning observation [13].

Differential BDS (D-BDS) uses at least one reference station with known position to correct the error of satellite signal and improve the positioning accuracy. The principle is that the reference station receives signals from satellites. Since the precise position of the reference station is known, it can calculate the error of each satellite signal, including

satellite orbit error, ionosphere and troposphere delay error. These error information is then sent to nearby user devices in real time through a communication method (such as radio). After the user equipment receives the differential signal, the error information is used to correct the satellite signal received by the user equipment to achieve more accurate position determination. [14] The principle diagram of RTK technology is shown in Figure 2.

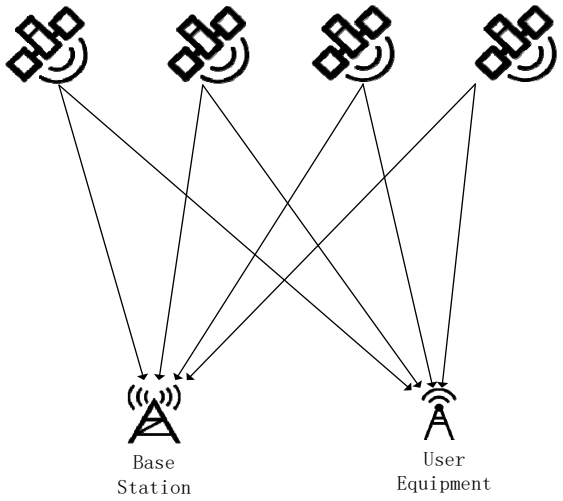

Fig 2. BeiDou satellite differential positioning schematic diagram

3. Inertial Navigation System

Inertial navigation system is a system that uses accelerometers and gyroscopes in inertial measurement units to measure and calculate the position, velocity, and attitude angle of the carrier. The gyroscope is responsible for measuring the angular velocity of the carrier in each axial direction. These data can be used to calculate the attitude angle of the carrier. The accelerometer provides the measurement of the acceleration of the carrier in space. The measurement results can be processed by time integration to derive the velocity change and position offset of the carrier. The inertial navigation system does not depend on the external reference signal and can work independently in any environment.

The inertial navigation system uses a series of inertial measurement devices and complex navigation algorithms to provide accurate position, velocity and attitude information for the device. The key challenge of inertial navigation system is to deal with the inevitable cumulative drift error in long-term operation, especially the error from gyroscope. This error is due to the fact that the angular velocity measured by the gyroscope needs to be converted into position and velocity information through integration. The error will accumulate over time and affect the positioning accuracy. In order to optimize the performance of INS, it is very important to take measures to correct the drift error. The main correction methods include internal self-correction and external auxiliary correction. Internal self-correction compensates the drift error of the gyroscope by analyzing the accelerometer data, and adjusts and corrects the gyroscope data by using the static or dynamic acceleration signal detected by the accelerometer. External auxiliary correction performs comprehensive error correction by integrating external positioning technologies, such as global positioning systems. The external position information provided by GPS can be used to periodically correct the error caused by drift in INS, and significantly improve the positioning accuracy of long-term operation [15].

$$R = \begin{bmatrix} a_1^T a_1' & a_1^T a_2' & a_1^T a_3' \\ a_2^T a_1' & a_2^T a_2' & a_2^T a_3' \\ a_3^T a_1' & a_3^T a_2' & a_3^T a_3' \end{bmatrix} \tag{2}$$

In three-dimensional Euclidean space, the rotation of a rigid body can be described by two mathematical methods : rotation matrix and rotation vector. The rotation matrix can accurately represent the rotation action of the object in space through the form of linear transformation, and the rotation vector shows the rotation axis and its rotation angle in an intuitive way. Each rotation can be uniquely described by a determined rotation axis and rotation angle. Assuming the unit vector is denoted as n and the rotation vector is represented as $\theta = \theta n$, the corresponding rotation matrix can be derived using Rodrigues' rotation formula:

$$R = \cos\theta I + (1-\cos\theta) n n^T + \sin\theta n^{\wedge} \tag{3}$$

Here, $n^{\wedge}$ denotes the skew-symmetric matrix associated with the vector n.

$$n^{\wedge} = \begin{bmatrix} 0 & -n_3 & n_2 \\ n_3 & 0 & -n_1 \\ -n_2 & n_1 & 0 \end{bmatrix} \tag{4}$$

Conversely, the conversion formula from a rotation matrix to a rotation vector is given by:

$$\begin{cases} \theta = \arccos \dfrac{\mathrm{t}r(R)-1}{2} \\ Rn = n \end{cases} \tag{5}$$

Where n is the eigenvector corresponding to the eigenvalue of 1.

Compared with the rotation matrix and rotation vector, Euler angle provides a more intuitive description of rotation, which expresses the overall rotation by rotating independently around three mutually perpendicular axes. [17] A major feature of this representation is that the same rotation can be achieved by different combinations of Euler angles, showing its non-uniqueness. The expression of Euler angle is divided into two categories : internal rotation and external rotation. In the internal rotation mode, the rotation is relative to the coordinate axis of the object itself, while in the external rotation mode, the rotation is relative to the fixed external reference frame. The same set of Euler angles can be rotated according to different axis sequences, resulting in different results. Generally, the Euler angle is represented by yaw angle, pitch angle and roll angle, and the internal rotation strategy is adopted. The rotation order is ZYX, that is, the yaw angle is first rotated around the Z axis, followed by the pitch angle of the Y axis, and finally the roll angle of the X axis. Let $\begin{bmatrix} \alpha & \beta & \gamma \end{bmatrix}$ represent the yaw, pitch, and roll angles, respectively. The corresponding rotation matrices can be expressed as:

$$
\begin{aligned}
&R_{ZYX}(\alpha,\beta,\gamma) = R_Z(\alpha)R_Y(\beta)R_X(\gamma) \\
&= \begin{bmatrix} \cos\alpha & -\sin\alpha & 0 \\ \sin\alpha & \cos\alpha & 0 \\ 0 & 0 & 1 \end{bmatrix} \begin{bmatrix} \cos\beta & 0 & \sin\beta \\ 0 & 1 & 0 \\ -\sin\beta & 0 & \cos\beta \end{bmatrix} \begin{bmatrix} 1 & 0 & 0 \\ 0 & \cos\gamma & -\sin\gamma \\ 0 & \sin\gamma & \cos\gamma \end{bmatrix} \\
&= \begin{bmatrix} \cos\alpha\cos\beta & \cos\alpha\sin\beta\sin\gamma - \sin\alpha\cos\gamma & \cos\alpha\sin\beta\cos\gamma + \sin\alpha\sin\gamma \\ \sin\alpha\cos\beta & \sin\alpha\sin\beta\sin\gamma + \cos\alpha\cos\gamma & \sin\alpha\sin\beta\cos\gamma - \cos\alpha\sin\gamma \\ -\sin\beta & \cos\beta\sin\gamma & \cos\beta\cos\gamma \end{bmatrix}
\end{aligned} \tag{6}
$$

When the Euler angle is used to describe the rotation, the so-called ' universal lock ' phenomenon will be encountered, which means that the system may lose a rotation degree of freedom in a specific rotation state, resulting in different angle combinations that can represent the same rotation attitude. This feature makes the Euler angle impractical in situations that require continuity and consistency (such as filtering and optimization algorithms), because it may produce sudden jumps or discontinuities during interpolation and conversion [18]. Therefore, although the Euler angle is very effective in providing users with intuitive rotation descriptions and is usually more suitable for human-computer interaction environments, its application in technical calculations and dynamic simulations is limited.

In contrast, quaternions, as a mathematical tool for representing and calculating rotations in three-dimensional space, avoid the ' universal lock ' problem, and provide a more stable and efficient way to handle three-dimensional rotations. It can represent any rotation without worrying about the loss of degrees of freedom. [19]

A quaternion consists of one real component and three imaginary components:

$$
q = q_0 + q_1 i + q_2 j + q_3 k = [q_0, q_1, q_2, q_3]^T = [s, v]^T \tag{7}
$$

The relationship among the three imaginary components is defined as follows:

$$
\begin{cases} i^2 = j^2 = k^2 = -1 \\ ij = k, ji = -k \\ jk = i, kj = -i \\ ki = j, ik = -j \end{cases} \tag{8}
$$

Quaternion is a method to express three-dimensional rotation. Each rotation in three-dimensional space can be uniquely represented by a specific unit quaternion, which can avoid the singularity in rotation vector and Euler angle representation.

Calculations for quaternion addition, subtraction, scalar multiplication, and multiplication:

$$
q_a \pm q_b = [s_a \pm s_b, v_a \pm v_b]^T \tag{9}
$$

$$
\lambda q_a = [\lambda s, \lambda v]^T \tag{10}
$$

$$
q_a \otimes q_b = [s_a s_b - {v_a}^T v_b, s_a v_b + s_b v_a + v_a \times v_b]^T \tag{11}
$$

Conversion of quaternion multiplication into matrix multiplication:

$$
q_a \otimes q_b = Q_L(q_a) q_b = Q_R(q_b) q_a \tag{12}
$$

Q_L and Q_{R} represent the left-multiplication matrix and the right-multiplication matrix of a quaternion, respectively:

$$
Q_L(q) = sI + \begin{bmatrix} 0 & -v^T \\ v & v^{\wedge} \end{bmatrix} \tag{13}
$$

$$
Q_R(q) = sI + \begin{bmatrix} 0 & -v^T \\ v & v^{\wedge} \end{bmatrix} \tag{14}
$$

The norm (or magnitude) of a quaternion:

$$
q = \sqrt{q_0^2 + q_1^2 + q_2^2 + q_3^2} \tag{15}
$$

The conjugate of a quaternion:

$$
q^* = [s, -v]^T \tag{16}
$$

Self-multiplication of a quaternion:

$$
q^* \otimes q = q \otimes q^* = [s^2 + v^T v, 0]^T \tag{17}
$$

When representing rotations with quaternions, a three-dimensional point $p = [0, x, y, z]^T$ rotated by a quaternion \$q\$ can be expressed as:

$$
p' = qpq^{-1} \tag{18}
$$

When converting between a quaternion and a rotation vector, a given rotation vector can be represented in quaternion form as:

$$
q = \left[\cos\frac{\theta}{2}, n_x \sin\frac{\theta}{2}, n_y \sin\frac{\theta}{2}, n_z \sin\frac{\theta}{2} \right]^T \tag{19}
$$

Similarly, when parameterizing rotation utilizing a quaternion:

$$
\theta = 2\arccos q_0 \tag{20}
$$

$$
n = \frac{v}{\sin\frac{\theta}{2}} \tag{21}
$$

4. Extended Kalman Filter

Kalman filter, also known as linear quadratic estimation, is an efficient recursive filtering algorithm specially designed to accurately estimate the state of a dynamic system from a series of noisy data measurements. It is based on the analysis of a series of observation data containing statistical noise and external system interference to provide accurate estimation of the system state. Compared with the method that relies only on a single measurement result, Kalman filter can provide more accurate estimation. [20].

The core idea of Kalman filter is to fuse prior knowledge and real-time measurement to estimate the current state of the system, and use each new measurement data to continuously update and correct the estimated value. This process mainly

includes two stages : prediction stage and update stage. Kalman filtering technology shows its advantages of fast, accurate and real-time processing in the field of data filtering and state estimation due to its simplicity of mathematical model and easy programming. This algorithm is widely used in many fields, including communication, navigation, guidance and control systems, and has become one of the most widely used data processing algorithms. Although Kalman filtering has obvious advantages in terms of processing efficiency and simplified calculation, it is mainly oriented to the application scenarios of linear Gaussian models, which limits its application in nonlinear systems. [21]

In practical applications, the state transition and observation models of many dynamic systems are nonlinear. For example, the systems involved in agricultural machinery automatic navigation are often nonlinear systems, which makes the standard Kalman filter unable to be directly applied. [22]. Extended Kalman Filter (EKF), as a variant of Kalman filter, is specially designed to deal with state estimation involving nonlinear models. The core strategy of EKF is to perform linearization on the nonlinear model. This process applies Taylor series expansion to the model at each moment to achieve local linearization of the model, so that the theoretical framework of Kalman filter can be applied in the state estimation of nonlinear systems [23].

Assuming that the state transition and observation models of a dynamic system are represented by non-linear functions $f(\cdot)$ and $h(\cdot)$, respectively, the state transition and observation models can be formulated as:

$$\begin{cases} x_k = f\left(x_{k-1}, u_k\right) + w_k \\ z_k = h\left(x_k\right) + v_k \end{cases} \tag{22}$$

Here, $\mathbf{x}_k$ represents the state vector at time k, $\mathbf{x}_{k-1}$ denotes the state at time $k-1$, and $\mathbf{z}_k$ signifies the measurement vector at time k. The crucial mechanism of the Extended Kalman Filter (EKF) in processing non-linear systems lies in performing a Taylor series expansion on the non-linear functions $f(\cdot)$ and $h(\cdot)$ around the most recent state estimate. The original functions are thereby substituted with their first-order linear approximations, which can be expressed as:

$$x_k = f\left(\hat{x}_{k-1}\right) + F_{k-1}\left(x_{k-1} - \hat{x}_{k-1}\right) + w_k \tag{23}$$

$$z_k = h\left(\hat{x}_k\right) + H_k\left(x_k - \hat{x}_k\right) + v_k \tag{24}$$

Here, $\mathbf{w}_{k-1}$ and $\mathbf{v}_k$ represent the process noise and the observation noise, respectively. The linearization is primarily achieved by computing the Jacobian matrices of the functions $f(\cdot)$ and $h(\cdot)$ at the specified estimation points:

$$F_{k-1} = \left.\frac{\partial f}{\partial x}\right|_{\hat{x}_{k-1}} \qquad H_k = \left.\frac{\partial h}{\partial x}\right|_{\hat{x}_k} \tag{25}$$

The Extended Kalman Filter (EKF) is primarily composed of two distinct phases: prediction and update. In the prediction phase, the current state estimate is utilized to forecast the subsequent state along with its associated uncertainty (represented by the error covariance).

State prediction:

$$\hat{x}_k' = f\left(\hat{x}_{k-1}\right) \tag{26}$$

Error covariance prediction:

$$P_k' = F_{k-1} P_{k-1} F_{k-1}^{\mathrm{T}} + Q_k \tag{27}$$

Where $\mathbf{Q}_k$ is the process noise covariance matrix, representing the uncertainty inherent in the process.

The state update process of the Extended Kalman Filter (EKF) incorporates new observation information into the current state prediction to correct the predicted state and error covariance. The formulas are as follows:

The Kalman Gain:

$$K_k = P_k' H_k^{\mathrm{T}} \left(H_k P_k' H_k^{\mathrm{T}} + R\right)^{-1} \tag{28}$$

State update:

$$\hat{x}_k = \hat{x}_k' + K_k\left(z_k - H_k \hat{x}_k'\right) \tag{29}$$

Error covariance update:

$$P_k = \left(I - K_k H_k\right) P_k' \tag{30}$$

Where the Kalman gain represents the weight of the observation data relative to the predicted state, and R denotes the measurement noise covariance matrix.

5. Visual/Inertial/Satellite Extended Kalman Filter

5.1. Prediction Model

The automatic navigation information provided by visual navigation to agricultural machinery is mainly lateral position deviation and heading angle deviation. The lateral position can provide the lateral distance between the position of agricultural machinery camera and the navigation line of farmland. The heading angle provides the angle between the camera and the navigation line, which can realize the automatic navigation of agricultural machinery to a certain extent. Considering the limitations of visual navigation, such as camera occlusion, signal distortion, etc., this section will introduce GNSS and IMU observations on the basis of visual navigation to design an extended Kalman filter.

The state variables and control variables of the filter are designed as:

$$\begin{aligned} \mathbf{x} &= \left[\mathbf{q}, \mathbf{g_b}, \mathbf{a_b}, d, \theta, \mathbf{p}, \mathbf{v}\right]^{\mathbf{T}} \\ &= \left[q_w, q_x, q_y, q_z, g_{b_x}, g_{b_y}, g_{b_z}, a_{b_x}, a_{b_y}, a_{b_z}, d, \theta, p_n, p_e, p_d, v_n, v_e, v_d\right]^{\mathbf{T}} \end{aligned} \tag{31}$$

Where q denotes the quaternion, g_b represents the gyroscope bias, a_b is the accelerometer bias, d indicates the lateral position deviation, θ stands for the heading angle deviation, p refers to the GNSS position, and v denotes the velocity.

The state transition process is formulated as:

$$f(x_k)=\begin{bmatrix}\mathbf{q}_k\\ \mathbf{g}_{\mathbf{b}_k}\\ \mathbf{a}_{\mathbf{b}_k}\\ d_k\\ \theta_k\\ p_k\\ v_k\end{bmatrix}=\begin{bmatrix}\mathbf{q}_{k-1}\otimes\begin{bmatrix}1\\ \frac{1}{2}\bar{\hat{\boldsymbol{\omega}}}_{k-1}\delta t\end{bmatrix}\\ g_{b_{k-1}}\\ a_{b_{k-1}}\\ d\\ \theta_{k-1}+\begin{bmatrix}0\\0\\1\end{bmatrix}^T\mathbf{R}^w_{b_{k-1}}\bar{\hat{\boldsymbol{\omega}}}_{k-1}\delta t\\ p_{k-1}+\bar{\hat{\mathbf{v}}}_{k-1}\delta t\\ v_{k-1}+\mathbf{R}^w_{b_{k-1}}\bar{\hat{\mathbf{m}}}_{k-1}\delta t\end{bmatrix}+\mathbf{w}_k \tag{32}$$

Where δt denotes the state update period, $\mathbf{R}^w_{b_{k-1}}$ represents the rotation from the body frame to the inertial frame, $\bar{\hat{\boldsymbol{\omega}}}_{k-1}$ is the mid-point integration of the gyroscope, and $\bar{\hat{\mathbf{m}}}_{k-1}$ is the mid-point integration of the accelerometer.

$$\bar{\hat{\boldsymbol{\omega}}}_{k-1}=\frac{\boldsymbol{\omega}_{k-1}+\boldsymbol{\omega}_k}{2}-\mathbf{g}_{b_{k-1}} \tag{33}$$

$$\bar{\hat{\mathbf{m}}}_{k-1}=\frac{\mathbf{m}_{k-1}+\mathbf{m}_k}{2}-\mathbf{a}_{b_{k-1}} \tag{34}$$

The Jacobian matrix, obtained by differentiating the state transition function with respect to each state variable, is given by:

$$\mathbf{F}_{k-1}=\frac{\partial\mathbf{f}(\mathbf{x}_k)}{\partial\mathbf{x}_{k-1}}=\begin{bmatrix}\mathbf{I}+\frac{1}{2}\mathrm{Q}_R\left(\begin{bmatrix}0\\ \bar{\hat{\boldsymbol{\omega}}}\end{bmatrix}\right)\delta t & -\frac{1}{2}\mathrm{Q}_L(\mathbf{q}_{k-1})\begin{bmatrix}\mathbf{0}\\ \mathbf{I}_{3\times3}\end{bmatrix}\delta t & \mathbf{0}_{4\times3} & \mathbf{0}_{4\times2} & \mathbf{0}_{4\times3} & \mathbf{0}_{4\times3}\\ \mathbf{0}_{3\times4} & \mathbf{I}_{3\times3} & \mathbf{0}_{3\times3} & \mathbf{0}_{3\times2} & \mathbf{0}_{3\times3} & \mathbf{0}_{3\times3}\\ \mathbf{0}_{3\times4} & \mathbf{0}_{3\times3} & \mathbf{I}_{3\times3} & \mathbf{0}_{3\times2} & \mathbf{0}_{3\times3} & \mathbf{0}_{3\times3}\\ \mathbf{F}_{k-1}(d,\theta;\mathbf{q}_k) & \mathbf{F}_{k-1}(d,\theta;\mathbf{b}_{\mathbf{g}_{k-1}}) & \mathbf{0}_{2\times3} & \mathbf{I}_{2\times2} & \mathbf{0}_{2\times3} & \mathbf{0}_{2\times3}\\ \mathbf{0}_{3\times4} & \mathbf{0}_{3\times3} & \mathbf{0}_{3\times3} & \mathbf{0}_{3\times2} & \mathbf{I}_{3\times3} & \mathbf{v}_{k-1}[\mathbf{I}_{3\times3}]\delta t\\ \mathbf{F}_{k-1}(v;\mathbf{q}_k) & \mathbf{0}_{3\times3} & \mathbf{F}_{k-1}(v;a_k) & \mathbf{0}_{3\times2} & \mathbf{0}_{3\times3} & \mathbf{I}_{3\times3}\end{bmatrix} \tag{35}$$

$$\begin{aligned}\mathbf{F}_{k-1}(d,\theta;\mathbf{q}_k)&=2\delta t\begin{bmatrix}0 & 0 & 0\\ 2q_{w_{k-1}}q_{y_{k-1}}-2q_{x_{k-1}}q_{z_{k-1}} & 2q_{w_{k-1}}q_{x_{k-1}}+2q_{y_{k-1}}q_{z_{k-1}} & 2q^2_{x_{k-1}}+2q^2_{y_{k-1}}-1\end{bmatrix}\\ &=\begin{bmatrix}0 & 0 & 0 & 0\\ q_{x_{k-1}}\bar{\hat{\boldsymbol{\omega}}}_{y_{k-1}}-q_{y_{k-1}}\bar{\hat{\boldsymbol{\omega}}}_{x_{k-1}} & q_z\bar{\hat{\boldsymbol{\omega}}}_{y_{k-1}}+q_w\bar{\hat{\boldsymbol{\omega}}}_{y_{k-1}}-2q_x\bar{\hat{\boldsymbol{\omega}}}_{z_{k-1}} & q_z\bar{\hat{\boldsymbol{\omega}}}_{y_{k-1}}-q_w\bar{\hat{\boldsymbol{\omega}}}_{y_{k-1}}-2q_x\bar{\hat{\boldsymbol{\omega}}}_{z_{k-1}} & q_x\bar{\hat{\boldsymbol{\omega}}}_{x_{k-1}}+q_y\bar{\hat{\boldsymbol{\omega}}}_{y_{k-1}}\end{bmatrix}\end{aligned} \tag{36}$$

$$\mathbf{F}_{k-1}(d,\theta;\mathbf{g}_{b_{k-1}})=\delta t\begin{bmatrix}0 & 0 & 0\\ 2q_{w_{k-1}}q_{y_{k-1}}-2q_{x_{k-1}}q_{z_{k-1}} & 2q_{w_{k-1}}q_{x_{k-1}}+2q_{y_{k-1}}q_{z_{k-1}} & 2q^2_{x_{k-1}}+2q^2_{y_{k-1}}-1\end{bmatrix} \tag{37}$$

$$\mathbf{F}_{k-1}(v;q_k)=2\delta t\begin{bmatrix}q_{w_{k-1}}\bar{\hat{\mathbf{m}}}_{x_{k-1}}-q_{z_{k-1}}\bar{\hat{\mathbf{m}}}_{y_{k-1}}+q_{y_{k-1}}\bar{\hat{\mathbf{m}}}_{z_{k-1}} & q_{x_{k-1}}\bar{\hat{\mathbf{m}}}_{x_{k-1}}+q_{y_{k-1}}\bar{\hat{\mathbf{m}}}_{y_{k-1}}+q_{z_{k-1}}\bar{\hat{\mathbf{m}}}_{z_{k-1}} & q_{x_{k-1}}\bar{\hat{\mathbf{m}}}_{y_{k-1}}-q_{y_{k-1}}\bar{\hat{\mathbf{m}}}_{x_{k-1}}+q_{w_{k-1}}\bar{\hat{\mathbf{m}}}_{z_{k-1}} & -q_{z_{k-1}}\bar{\hat{\mathbf{m}}}_{x_{k-1}}+q_{x_{k-1}}\bar{\hat{\mathbf{m}}}_{y_{k-1}}-q_{x_{k-1}}\bar{\hat{\mathbf{m}}}_{z_{k-1}}\\ q_{z_{k-1}}\bar{\hat{\mathbf{m}}}_{x_{k-1}}+q_{w_{k-1}}\bar{\hat{\mathbf{m}}}_{y_{k-1}}-q_{x_{k-1}}\bar{\hat{\mathbf{m}}}_{z_{k-1}} & q_{x_{k-1}}\bar{\hat{\mathbf{m}}}_{y_{k-1}}-q_{y_{k-1}}\bar{\hat{\mathbf{m}}}_{x_{k-1}}+q_{w_{k-1}}\bar{\hat{\mathbf{m}}}_{z_{k-1}} & q_{x_{k-1}}\bar{\hat{\mathbf{m}}}_{x_{k-1}}+q_{y_{k-1}}\bar{\hat{\mathbf{m}}}_{y_{k-1}}+q_{z_{k-1}}\bar{\hat{\mathbf{m}}}_{z_{k-1}} & q_{w_{k-1}}\bar{\hat{\mathbf{m}}}_{x_{k-1}}-q_{z_{k-1}}\bar{\hat{\mathbf{m}}}_{y_{k-1}}+q_{y_{k-1}}\bar{\hat{\mathbf{m}}}_{z_{k-1}}\\ q_{x_{k-1}}\bar{\hat{\mathbf{m}}}_{y_{k-1}}-q_{y_{k-1}}\bar{\hat{\mathbf{m}}}_{x_{k-1}}+q_{x_{k-1}}\bar{\hat{\mathbf{m}}}_{z_{k-1}} & q_{z_{k-1}}\bar{\hat{\mathbf{m}}}_{x_{k-1}}+q_{w_{k-1}}\bar{\hat{\mathbf{m}}}_{y_{k-1}}-q_{x_{k-1}}\bar{\hat{\mathbf{m}}}_{z_{k-1}} & q_{w_{k-1}}\bar{\hat{\mathbf{m}}}_{x_{k-1}}-q_{z_{k-1}}\bar{\hat{\mathbf{m}}}_{y_{k-1}}+q_{y_{k-1}}\bar{\hat{\mathbf{m}}}_{z_{k-1}} & q_{x_{k-1}}\bar{\hat{\mathbf{m}}}_{x_{k-1}}+q_{y_{k-1}}\bar{\hat{\mathbf{m}}}_{y_{k-1}}+q_{z_{k-1}}\bar{\hat{\mathbf{m}}}_{z_{k-1}}\end{bmatrix} \tag{38}$$

$$\mathbf{F}_{k-1}(v;a_k)=\delta t\begin{bmatrix}q^2_{w_{k-1}}+q^2_{x_{k-1}}-q^2_{y_{k-1}}-q^2_{z_{k-1}} & -2q_{w_{k-1}}q_{z_{k-1}}+2q_{x_{k-1}}q_{y_{k-1}} & 2q_{w_{k-1}}q_{y_{k-1}}+2q_{x_{k-1}}q_{z_{k-1}}\\ 2q_{w_{k-1}}q_{z_{k-1}}+2q_{x_{k-1}}q_{y_{k-1}} & q^2_{w_{k-1}}-q^2_{x_{k-1}}+q^2_{y_{k-1}}-q^2_{z_{k-1}} & -2q_{w_{k-1}}q_{x_{k-1}}+2q_{y_{k-1}}q_{z_{k-1}}\\ 2q_{w_{k-1}}q_{y_{k-1}}-2q_{x_{k-1}}q_{z_{k-1}} & 2q_{w_{k-1}}q_{x_{k-1}}+2q_{y_{k-1}}q_{z_{k-1}} & q^2_{w_{k-1}}-q^2_{x_{k-1}}-q^2_{y_{k-1}}+q^2_{z_{k-1}}\end{bmatrix} \tag{39}$$

5.2. Observation Model

The observation variables of the filter are designed as:

$$\begin{aligned}\mathbf{z}&=[\mathbf{a},d,\theta,\mathbf{p}]^{\mathrm{T}}\\ &=[a_x,a_y,a_z,d,\theta,p_n,p_e,p_d]^{\mathrm{T}}\end{aligned} \tag{40}$$

Where (a_x,a_y,a_z) represents the three-axis acceleration measurements provided by the IMU. d and θ denote the lateral position deviation and heading angle deviation observed by the vision system, respectively. (p_n,p_e,p_d) indicates the latitude, longitude, and altitude

coordinates provided by the GNSS.

Since the observation system is a discretized process, the observation model is formulated as:

$$h_k(x_k)=\begin{bmatrix} a_k \\ d \\ \theta \\ p \end{bmatrix}=\begin{bmatrix} \mathbf{R}^b_{w_k}\begin{bmatrix}0\\0\\1\end{bmatrix} \\ d_k \\ \theta_k \\ p_k \end{bmatrix}+v_k \tag{41}$$

By differentiating the observation function with respect to the state variables, the observation Jacobian matrix is obtained as:

$$H_k=\frac{\partial h(x_k)}{\partial x_k}=\begin{bmatrix} H_k(a^b;q_k) & 0_{3\times6} & 0_{3\times5} & 0_{3\times3} \\ 0_{5\times4} & & 0_{5\times6} & I_{5\times5} & 0_{5\times3} \end{bmatrix} \tag{42}$$

$$H_k(a^b;q_k)=\begin{bmatrix} -2q_y & 2q_z & -2q_w & 2q_x \\ 2q_x & 2q_w & 2q_z & 2q_y \\ 2q_w & 2q_x & -2q_y & 2q_z \end{bmatrix} \tag{43}$$

$$\begin{aligned} R^b_w &= R^{bT}_w = R_{zxy}(\phi)^T \\ &= \begin{bmatrix} \cos\phi_y\cos\phi_z-\sin\phi_y\sin\phi_x\sin\phi_z & -\cos\phi_x\sin\phi_z & \sin\phi_y\cos\phi_z+\cos\phi_y\sin\phi_x\sin\phi_z \\ \cos\phi_y\sin\phi_z+\sin\phi_y\sin\phi_x\cos\phi_z & -\cos\phi_x\sin\phi_z & \cos\phi_y\cos\phi_z-\sin\phi_y\sin\phi_x\sin\phi_z \\ -\sin\phi_y\cos\phi_x & \sin\phi_x & \cos\phi_y\cos\phi_x \end{bmatrix} \end{aligned} \tag{44}$$

Therefore:

$$\phi_x=\arcsin(\bar{a}_y,\sqrt{\bar{a}_x{}^2+\bar{a}_z{}^2}) \tag{45}$$

$$\phi_y=\text{-}\operatorname{atan}2(\bar{a}_x,\bar{a}_z) \tag{46}$$

After placing the IMU on a flat and stable surface, the yaw angle can be determined from the magnetometer measurements. If the magnetometer reading is denoted as $\mathbf{m}=\begin{bmatrix} m_x,m_y,m_z \end{bmatrix}^T$, the calculation formula for the yaw angle is given by:

$$\phi_z=\operatorname{atan}2(m_y,m_x) \tag{47}$$

The conversion of the initial Euler angles into a quaternion is formulated as follows:

$$\begin{aligned} q_0=q_z\otimes q_x\otimes q_y &= \begin{bmatrix}\cos\frac{\phi_z}{2}\\0\\0\\\cos\frac{\phi_z}{2}\end{bmatrix}\otimes\begin{bmatrix}\cos\frac{\phi_x}{2}\\\cos\frac{\phi_x}{2}\\0\\0\end{bmatrix}\otimes\begin{bmatrix}\cos\frac{\phi_x}{2}\\0\\\sin\frac{\phi_x}{2}\\0\end{bmatrix} \\ &= \begin{bmatrix} \cos\frac{\phi_x}{2}\cos\frac{\phi_y}{2}\cos\frac{\phi_z}{2}-\sin\frac{\phi_x}{2}\sin\frac{\phi_y}{2}\sin\frac{\phi_z}{2} \\ \sin\frac{\phi_x}{2}\cos\frac{\phi_y}{2}\cos\frac{\phi_z}{2}-\cos\frac{\phi_x}{2}\sin\frac{\phi_y}{2}\sin\frac{\phi_z}{2} \\ \cos\frac{\phi_x}{2}\sin\frac{\phi_y}{2}\cos\frac{\phi_z}{2}+\sin\frac{\phi_x}{2}\cos\frac{\phi_y}{2}\sin\frac{\phi_z}{2} \\ \cos\frac{\phi_x}{2}\cos\frac{\phi_y}{2}\sin\frac{\phi_z}{2}+\sin\frac{\phi_x}{2}\sin\frac{\phi_y}{2}\cos\frac{\phi_z}{2} \end{bmatrix} \end{aligned} \tag{48}$$

5.3. Filter Initialization

Initialization of the state variables:

In the initialization filter stage, the initial attitude needs to be set. This attitude is usually represented by Euler angle converted to quaternion. In the stationary state, the initial pitch and roll angles are estimated according to the reading of the accelerometer, and the initial yaw angle is initially calibrated according to the magnetometer.

$\bar{\mathbf{a}}=\begin{bmatrix}\bar{\mathbf{a}}_x,\bar{\mathbf{a}}_y,\bar{\mathbf{a}}_z\end{bmatrix}^{\mathbf{T}}$ represents the average acceleration measurement taken over a period when the robot is stationary.

$\bar{\mathbf{g}}=\begin{bmatrix}\bar{\mathbf{g}}_x,\bar{\mathbf{g}}_y,\bar{\mathbf{g}}_z\end{bmatrix}^{\mathbf{T}}$ represents the average angular velocity measurement taken over a period when the robot is stationary.

Where $\mathbf{g}=\begin{bmatrix}0,0,g\end{bmatrix}^{\mathbf{T}}$ represents the gravitational acceleration, R^b_w denotes the rotation from the inertial frame to the body frame, such that $\bar{\mathbf{a}}=R^b_w g$. $\phi=\begin{bmatrix}\phi_x,\phi_y,\phi_z\end{bmatrix}^{\mathbf{T}}$ represents the initial attitude Euler angles of the body; assuming a rotation sequence of "Z-X-Y", it yields:

The initial quaternion is calculated from the initial attitude angles, and the initial zero biases are obtained from the gyroscope and accelerometer readings under stationary conditions. The initial latitude and longitude coordinates are derived from stationary GNSS positioning, while the initial three-axis velocity is calibrated to zero. The lateral and heading deviations are obtained via image processing. Consequently, the initial state vector of the Extended Kalman Filter (EKF) is formulated as:

$$\mathbf{x}_0=\begin{bmatrix}\mathbf{q}_0,\mathbf{g}_{\mathbf{b}_0},\mathbf{a}_{\mathbf{b}_0},d_0,\theta_0,\mathbf{p}_0,\mathbf{v}_0\end{bmatrix}^{\mathbf{T}} \tag{49}$$

Initialization of Noise Covariance Matrices:

During the application of the Extended Kalman Filter (EKF) algorithm, the initial configuration involves defining the process noise covariance matrix and the measurement noise covariance matrix. These two matrices account for the inherent uncertainties within the system dynamics and the errors introduced during the measurement process, respectively. Given that this noise sources are mutually independent, both matrices are constructed as diagonal matrices.

The process noise covariance matrix is defined as:

$$Q_k=diag\begin{bmatrix}Q_g(\mathbf{q}_{k-1}),(w_{bg_x})^2,(w_{bg_y})^2,(w_{bg_z})^2,(w_{ba_x})^2,(w_{ba_y})^2,(w_{ba_z})^2, \\ (w_d)^2,(w_\theta)^2,(w_{p_x})^2,(w_{p_y})^2,(w_{p_z})^2,(w_{v_x})^2,(w_{v_y})^2,(w_{v_z})^2\end{bmatrix}^{\mathbf{T}} \tag{50}$$

$$Q_g(\mathbf{q}_{k-1})=\frac{1}{4}\delta t^2 Q_L(\mathbf{q}_{k-1})diag\begin{bmatrix}0,(w_{g_x})^2(w_{g_y})^2,(w_{g_z})^2\end{bmatrix}Q_L^T(\mathbf{q}_{k-1}) \tag{51}$$

Where *diag( )* denotes a diagonal matrix. Q_g represents

the rotation noise variance, $\left[w_{g_x}, w_{g_y}, w_{g_z} \right]$ represents the gyroscope noise variance, $\left[w_{bg_x}, w_{bg_y}, w_{bg_z} \right]$ denotes the gyroscope bias noise variance, and $\left[w_{ba_x}, w_{ba_y}, w_{ba_z} \right]$ indicates the accelerometer bias noise variance. w_d and w_θ represent the process noise variances for the lateral position and heading deviations of the visual navigation parameters, respectively. $\left[w_{p_x} w_{p_y}, w_{p_z} \right]$ stands for the GNSS positioning process noise variance, and $\left[w_{v_x}, w_{v_y}, w_{v_z} \right]$ denotes the process noise variance for the three-axis velocity estimation.

The observation noise covariance matrix is defined as:

$$R = diag\left[(v_{a_x})^2, (v_{a_y})^2, (v_{a_z})^2, (v_d)^2, (v_\theta)^2, (v_{p_x})^2, (v_{p_y})^2, (v_{p_z})^2 \right] \quad (52)$$

Where $\left[v_{a_x}, v_{a_y}, v_{a_z} \right]$ represents the accelerometer measurement noise; v_d and v_θ denote the measurement noise for the lateral position deviation and heading angle deviation of the visual navigation system, respectively; and $\left[v_{p_x}, v_{p_y}, v_{p_z} \right]$ indicates the GNSS positioning measurement noise.

The process error covariance matrix is an identity matrix, namely:

$$P_0 = I_{18\times18} \quad (53)$$

The process of the extended Kalman filter fusion algorithm is shown in Figure 4-1. The algorithm first uses IMU data to perform inertial navigation calculations to predict the future state of the device. The algorithm evaluates whether the latest GNSS data is available. When the GNSS data is reliable, EKF update is performed, and IMU and GNSS data are fused to accurately output position and attitude information. If the GNSS signal is missing or weak, the inertial solution will continue to be performed based on the previous state to maintain the continuous update of the position and attitude information. Similarly, the algorithm also relies on the path information from the computer vision system. When the path data is valid, it is combined with the IMU data to update the position and attitude through EKF. If the CV data is unreliable, the previous state is also used as the basis to continue to update the information according to the IMU. In the case of strong and reliable GNSS and CV data, the algorithm fuses the data of the three to achieve more accurate position and attitude updates. This fusion strategy aims to optimize the autonomous navigation ability of agricultural machinery and improve its positioning accuracy and stability in complex environments.

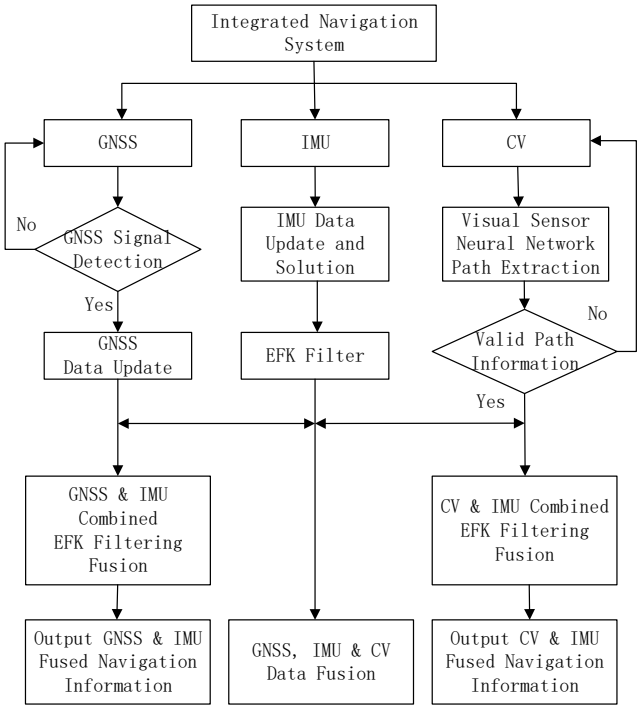

Fig 3. GNSS/CV/IMU multi-sensor data fusion

6. Simulation and Analysis

In this section, through Matlab simulation, the fusion navigation system combining computer vision, global navigation satellite system and inertial navigation system will be analyzed in depth to verify the effectiveness of the extended Kalman filter algorithm in improving the positioning accuracy of the system.

The simulation process is divided into the following steps : set up the hardware parameters and initial state of the INS inertial navigation system to generate navigation data including position and velocity information ; using satellite orbit data to estimate the position and velocity of the satellite and the receiver, and simulate the generation of GNSS data ; by constructing the visual navigation error model, the navigation parameter error is extracted ; according to the designed farmland driving trajectory, the Matlab toolbox is used to generate sensor data, and the EKF algorithm proposed

in this paper is used to perform data fusion, and the fused navigation data (including position, speed and attitude information) is evaluated. The sensor parameter deviation of the experimental simulation system is consistent with the actual selected hardware module parameter values. The simulation experiment parameter settings are detailed in table 1.

Table 1. Satellite/Inertial/Visual parameterization

IMU Parameters	Value	GNSS Parameters	Value	CV Parameters	Value
Gyroscope Gaussian noise	0.01°/s	GNSS position Gaussian white noise	0.3m	Lateral position random noise	0.02m
Gyroscope constant bias	8°/h	Sampling rate	10hz	Heading angle random noise	0.5°
Accelerometer Gaussian noise	0.01m/s²			Sampling rate	60hz
Accelerometer constant bias	0.06m/s²				
Sampling rate	100hz				

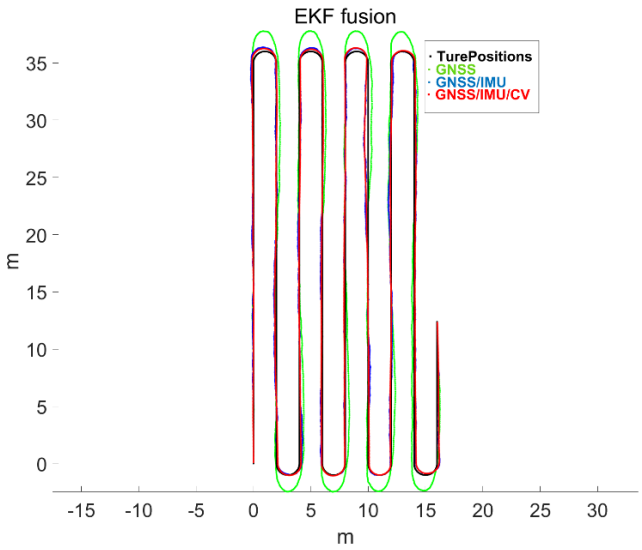

Fig 4. Matlab multi-sensor data fusion experiment

According to the above parameters, the model is established. The path is the conventional driving path of agricultural machinery. The driving length is 35 m, and the turning radius is 2.5 m. Matlab simulation is used. The path fusion results are shown in Figure 4, where the black path is the real path, the green path is EFK filtering using only GNSS, the blue path is GNSS and IMU extended Kalman filter fusion, and the red path is CV, GNSS and IMU extended Kalman filter fusion.

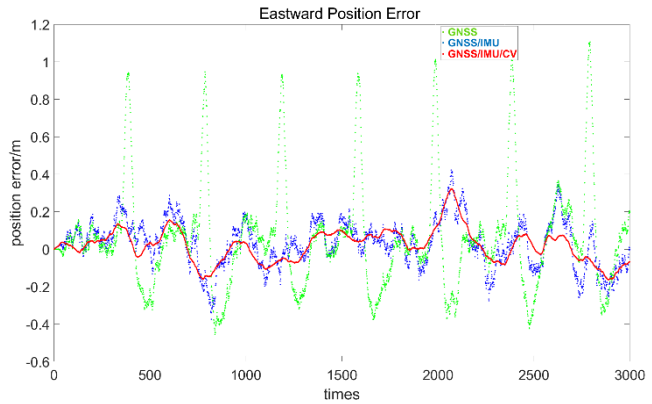

Fig 5. Eastward position error

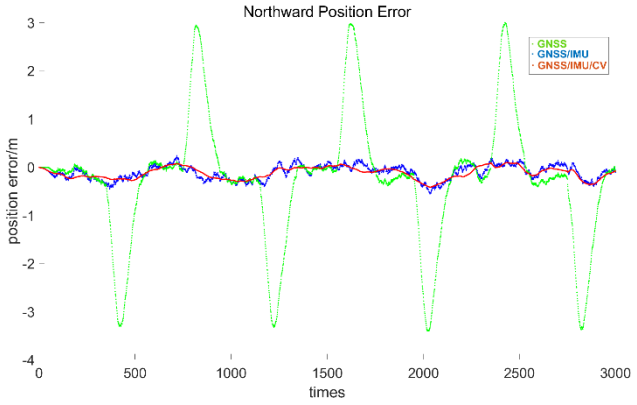

Fig 6. Northward position error

Figs.5 and 6 represent the position errors in the east and north directions, respectively. From Figure 4-3 and Figure 4-4, it can be seen that the integrated navigation system using satellite / inertial / visual multi-fusion after Kalman filtering, the east position error is in the range of − 0.42m ~ 0.37m, and the north position error is in the range of − 0.22m ~ 0.26m. Compared with single GNSS navigation and GNSS / IMU integrated navigation, the longitude error and dimension error are reduced after the introduction of visual update by extended Kalman filter. Especially in the case of complex motion at the end of the path, single GNSS navigation has a large error offset at the end of the path, and GNSS / IMU integrated navigation also has obvious fluctuations. It shows that the extended Kalman filter can be effectively applied to GNSS / IMU / CV in the integrated system, and the navigation accuracy is significantly improved.

By analyzing Figures 7 and 8, it can be seen that after Kalman filtering, the multi-sensor integrated navigation system (using satellite, inertial, and visual data) stabilizes the East velocity error between -1.12 m/s and 1.25 m/s, and the North velocity error between 1.12 m/s and 1.25 m/s. Compared to GNSS-only navigation, there is a significant improvement in velocity accuracy, especially in intervals with abrupt velocity changes. However, because the performance of the EKF is limited in highly non-linear systems, it conversely exhibits larger errors in intervals where the velocity is relatively stable.

Since the system model only uses CV and IMU data to update the heading angle, only CV and IMU are compared here. Through the analysis of Fig.9, it can be seen that the error fluctuation of the heading angle of the integrated

navigation system using inertial / visual fusion is very stable after Kalman filtering, and it is also stable between −4.2°~3.7° at the end of the turn. The introduction of IMU solves the problem of random error in visual navigation.

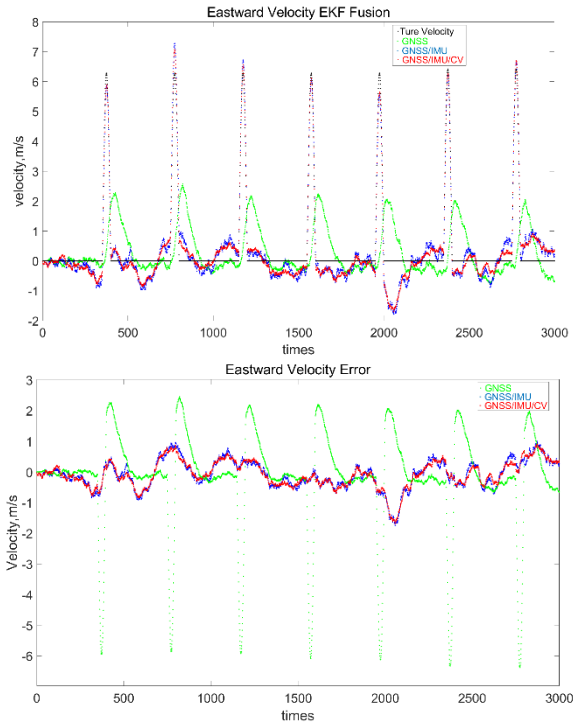

Fig 7. Eastward velocity fusion simulation and eastward velocity error

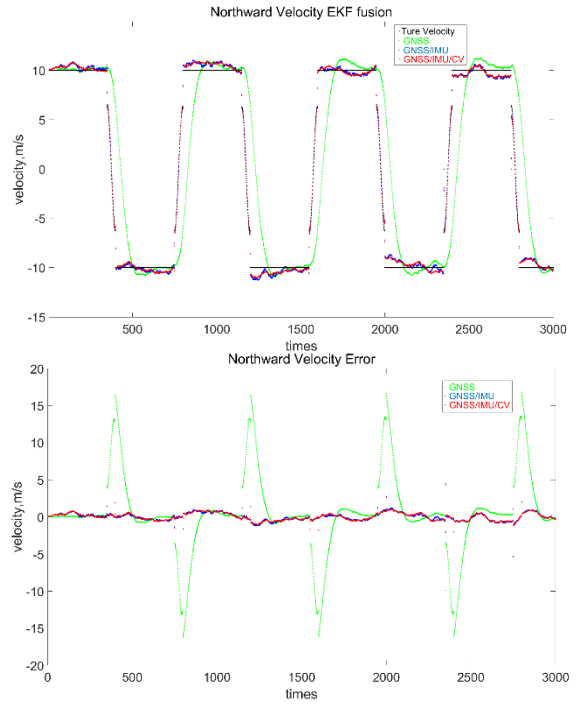

Fig 8. Northward velocity fusion simulation and northward velocity error

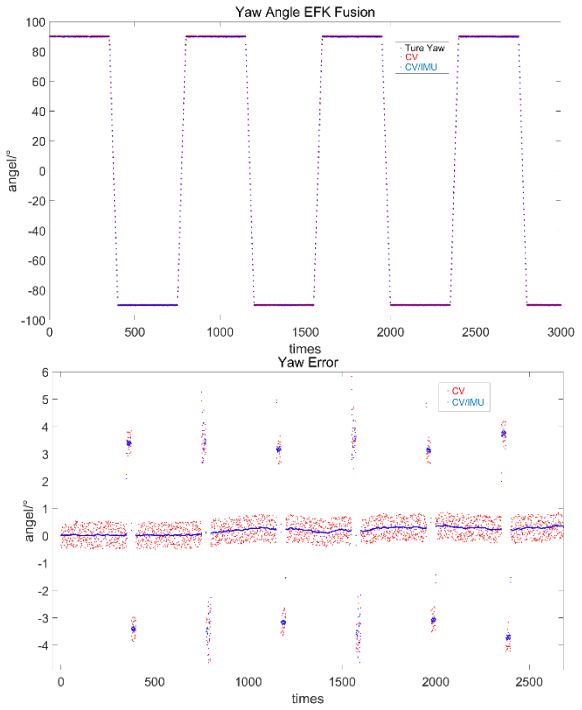

Fig 9. Yaw angle fusion simulation and heading angle error

7. Conclusion

In this paper, the application of extended Kalman filter algorithm in agricultural integrated navigation system is studied. The data processing flow of extended Kalman filter algorithm is deduced in detail. The integrated navigation system of GNSS, camera and inertial measurement unit is integrated by using extended Kalman filter technology. By synthesizing the characteristics of the above three sensors, the state equation is established based on 18-dimensional data of quaternion, triaxial acceleration, triaxial angular velocity, three-dimensional position, triaxial velocity, lateral deviation and angle deviation. Based on accelerometer data, GNSS positioning information and visual system output, as its observation update. By establishing a simulation model verification algorithm on Matlab, when only GNSS is used to update the observations, the maximum error in the east is − 0.6 to 1.2 meters, and the maximum error in the north is − 3.2 to 2.9 meters. After the introduction of IMU and CV updates, the maximum error in the east direction and the maximum error in the north direction reached − 0.3 to 0.4 meters and − 0.5 to 0.4 meters. The effective fusion of satellite / visual / inertial information is realized, the limitations of single sensor in various environments are solved, and the navigation accuracy is improved.

References

[1] Van Dinh, N., & Kim, G. W. (2020). Multi-sensor fusion towards VINS: A concise tutorial, survey, framework and challenges. In *2020 IEEE International Conference on Big Data and Smart Computing (BigComp)* (pp. 459–462). IEEE. https://doi.org/10.1109/BigComp48618.2020.00087.

[2] Wang, H., Li, D., Wu, C., & Yu, X. (2019). Depth perception of moving objects via structured light sensor with unstructured grid. *Results in Physics*, 13, 102163. https://doi.org/ 10. 1016/j.rinp.2019.102163.

[3] De Silva, V., Roche, J., & Kondoz, A. (2017). Fusion of LiDAR and camera sensor data for environment sensing in driverless vehicles. arXiv preprint arXiv:1707.07942.

[4] Delmerico, J., & Scaramuzza, D. (2018). A benchmark comparison of monocular visual-inertial odometry algorithms for flying robots. In *2018 IEEE International Conference on Robotics and Automation (ICRA)* (pp. 2502–2509). IEEE. https://doi.org/10.1109/ICRA.2018.8460552.

[5] Cadena, C., Carlone, L., Carrillo, H., Latif, Y., Scaramuzza, D., Neira, J., & Leonard, J. J. (2016). Past, present, and future of simultaneous localization and mapping: Toward the robust-perception age. *IEEE Transactions on Robotics*, 32(6), 1309–1332. https://doi.org/10.1109/TRO.2016.2624754.

[6] Sun, R., et al. (2020). Robust IMU/GPS/VO integration for vehicle navigation in GNSS degraded urban areas. *IEEE Sensors Journal*, 20(17), 10110–10122. https://doi.org/1 0. 1109/JSEN.2020.2992212.

[7] Reitbauer, E., & Schmied, C. (2021). Bridging GNSS outages with IMU and odometry: A case study for agricultural vehicles. *Sensors*, 21(13), 4467. https://doi.org/10.3390/s21134467.

[8] Zhang, G., & Hsu, L. T. (2018). Intelligent GNSS/INS integrated navigation system for a commercial UAV flight control system. *Aerospace Science and Technology*, 80, 368–380. https://doi.org/10.1016/j.ast.2018.07.029.

[9] Jing, Y., Li, Q., Ye, W., et al. (2023). Development of a GNSS/INS-based automatic navigation land levelling system. *Computers and Electronics in Agriculture*, 213, 108187. https://doi.org/10.1016/j.compag.2023.108187.

[10] Shalal, N., Low, T., McCarthy, C., et al. (2013). A review of autonomous navigation systems in agricultural environments. In *SEAg 2013: Innovative Agricultural Technologies for a Sustainable Future*.

[11] Demyanov, V. (2022). GNSS overview. In *Space Weather Impact on GNSS Performance* (pp. 5–87). Springer International Publishing. https://doi.org/10.1007/978-3-030-94502-6_2.

[12] Cheng, F., Feng, L., & Zhang, Y. (2004). The application of the Beidou Navigation System in marine hydrology and weather monitoring systems. *Journal of Ocean Technology*, 23(3), 70–73.

[13] Wang, J. B., Fang, S. S., Zhang, J. J., et al. (2017). Experimental analysis of BDS/GPS network differential positioning. *Science of Surveying and Mapping*, 42(4), 157–161.

[14] Li, Z., Yuan, Y., Fan, L., et al. (2013). Determination of the differential code bias for current BDS satellites. *IEEE Transactions on Geoscience and Remote Sensing*, 52(7), 3968–3979. https://doi.org/10.1109/TGRS.2013.2251916.

[15] Srinivas, P., & Kumar, A. (2017). Overview of architecture for GPS-INS integration. In *2017 Recent Developments in Control, Automation & Power Engineering (RDCAPE)* (pp. 433–438). IEEE. https://doi.org/10.1109/RDCAPE.2017.8276254.

[16] Ragozin, D. L. (1974). Rotation invariant measure algebras on Euclidean space. *Indiana University Mathematics Journal*, 23(12), 1139–1154. https://doi.org/10.1512/ iumj. 1974. 23. 121139.

[17] Henderson, D. M. (1977). Euler angles, quaternions, and transformation matrices for space shuttle analysis [Technical report].

[18] Zhao, X. Y., Wen, L. S., & Mei, C. L. (2012). Second-order kinematic singularity of attitude expressed by Eulerian angles. *Science Technology and Engineering*, 20(3), 634–637.

[19] Goldman, R. (2011). Understanding quaternions. *Graphical Models*, 73(2), 21–49. https://doi.org/ 10.1016/j. gmod. 2010. 12. 004.

[20] Welch, G., & Bishop, G. (1995). An introduction to the Kalman filter [Technical report].

[21] Kim, Y., & Bang, H. (2018). Introduction to Kalman filter and its applications. In *Introduction and Implementations of the Kalman Filter* (Vol. 1, pp. 1–16).

[22] Ribeiro, M. I. (2004). Kalman and extended Kalman filters: Concept, derivation and properties. *Institute for Systems and Robotics*, 43(46), 3736–3741.

[23] Barrau, A. (2015). Non-linear state error based extended Kalman filters with applications to navigation [Doctoral dissertation, Mines Paristech].